JOURNAL OF APPLIED ELECTROCHEMISTRY 11 (1981) 503–515

Optimization of an electrochemical hydrogen-chlorine energy storage system

K. L. HSUEH, D. -T. CHIN

Department of Chemical Engineering, Clarkson College of Technology, Potsdam, New York 13676, USA

J. MCBREEN, S. SRINIVASAN

Brookhaven National Laboratory, Department of Energy and Environment, Upton, New York 11973, USA

Received 26 September 1980

A mathematical model is presented for the optimization of the hydrogen–chlorine energy storage system. Numerical calculations have been made for a 20 MW plant being operated with a cycle of 10 h charge and 10 h discharge. Optimal operating parameters, such as electrolyte concentration, cell temperature and current densities, are determined to minimize the investment of capital equipment.

Nomenclature

A_{ex}	design heat transfer area of heat exchanger (m^2)
A_F	electrode area (m^2)
C_{p,Cl_2}	heat capacity of liquid chlorine ($J\,kg^{-1}\,K^{-1}$)
C_{v,H_2}	heat capacity of hydrogen gas at constant volume ($J\,kg^{-1}\,K^{-1}$)
$C_{p,HCl}$	heat capacity of aqueous HCl ($J\,kg^{-1}\,K^{-1}$)
$C_{\$acid}$	cost coefficient of HCl/Cl_2 storage ($\$\,m^{-1.4}$)
$C_{\$ex}$	cost coefficient of heat exchanger ($\$\,m^{-1.9}$)
$C_{\$F}$	cost coefficient of cell stack ($\$\,m^{-2}$)
$C_{\$H_2}$	cost coefficient of H_2 storage ($\$\,m^{-1.6}$)
$C_{\$j}$	cost coefficient of equipment j (\$/unit capacity)
$C_{\$pipe}$	cost coefficient of pipe ($\$\,m^{-1}$)
$C_{\$pump}$	cost coefficient of pump ($\$\,J^{-0.98}\,s^{-0.98}$)
E	cell voltage (V)
F	Faraday constant (9.65×10^7 C kg-equiv^{-1})
F_j	design capacity of equipment j (unit capacity)
G_D	design electrolyte flow rate ($m^3\,h^{-1}$)
H^0_{f,Cl_2}	heat of formation of liquid chlorine ($J\,kg\text{-}mol^{-1}\ Cl_2$)
$H^0_{f,HCl}$	heat of formation of aqueous HCl ($J\,kg\text{-}mol^{-1}$ HCl)
H_m	total mechanical energy losses (J)
I	total current flow through cell (A)
i	operating current density of cell stack ($A\,m^{-2}$)
L	length of pipeline (m)
N	number of parallel pipelines
Δn_{HCl}	change in the amount of HCl (kg-mole)
P	pressure of HCl/Cl_2 storage (kPa)
P_1	H_2 storage pressure at the beginning of charge (kPa)
P_2	H_2 storage pressure at the end of charge (kPa)
$-Q_{ex}$	heat removed through the heat exchanger (J)
R	universal gas constant ($8314\,J\,kg\text{-}mol^{-1}\,K^{-1}$)
S_{Cl_2}	the solubility of chlorine in aqueous HCl (kg-mole $Cl_2\,m^{-3}$ solution)
T	electrolyte temperature (K)
T_2	electrolyte temperature at the end of charge (K)
T_{max}	maximum electrolyte temperature (K)
T_{min}	minimum electrolyte temperature (K)

0021–891X/81/040503–13$03.30/0 © 1981 Chapman and Hall Ltd.

t	final time (h)
t_{ex}	the length of time for the heat exchanger operation (h)
U_{ex}	overall heat transfer coefficient ($J\,h^{-1}\,m^{-2}\,K^{-1}$)
V_{acid}	volume of HCl/Cl_2 storage (m^3)
V_{H_2}	volume of H_2 storage (m^3)
v	design linear velocity of electrolyte ($m\,s^{-1}$)
W_{Cl_2}	amount of liquid chloride at time t (kg)
$W_{Cl_2,0}$	amount of liquid chlorine at time t_0 (kg)
W_{HCl}	amount of aqueous HCl solution at time t (kg)
W_p	design brake power of pump ($J\,s^{-1}$)
X	electrolyte concentration of HCl at time t (wt fraction)
X_f	electrolyte concentration of HCl at the end of charge (wt fraction)
X_i	electrolyte concentration of HCl at the beginning of charge (wt fraction)
X_0	electrolyte concentration of HCl at time t_0 (wt fraction)
Y	objective function to be minimized ($\$\,kW^{-1}\,h^{-1}$)
α_j	the scale-up exponent of equipment j
ϵ	overall electric-to-electric efficiency (%)
ϵ_{acid}	safety factor of HCl/Cl_2 storage
ϵ_{Cl_2}	fractional excess of liquid chlorine
η_p	pump efficiency
$\bar{\rho}_{HCl}$	average density of HCl solution over the discharge period ($kg\,m^{-3}$)

1. Introduction

Since 1975, the hydrogen–chlorine cell has been considered for large-scale energy storage applications. An economic assessment of the system has been described [1] and nonsteady-state mass and heat balance [2] has been performed to identify the operating characteristics of the energy storage plant. It was found that an overall electric-to-electric energy conversion efficiency of greater than 70% could easily be achieved with this system. The system is based on a solid polymer electrolyte (SPE) cell. The properties of the cell membrane [3], the kinetics of electrode reactions, the cell construction, and the cell performance data [4] have been reported; the SPE technology allowed the cell to be operated at 3000 $A\,m^{-2}$ with small overvoltage losses. The technical feasibility of using a hydrogen–bromine cell [5] for energy storage has also been evaluated. This paper is concerned with a system optimization to minimize the capital investment of a 20 MW/200 MW h electrochemical hydrogen–chlorine energy storage plant designed to operate with a cycle of 10 h charge and 10 h discharge.

Optimization of battery systems has not been widely reported in the literature. Lucesoli and Degobert [6] optimized the performance of a hydrogen–air fuel cell to achieve a life span of 3000 h. Sharaevskii *et al.* [7] calculated the optimal amount of hydrophobic binder required in a gas-diffusion electrode. Ceynowa and Wodzki [8] used the simplex method to compute the optimal membrane thickness of a hydrogen–oxygen fuel cell. Brovalskii and Sinyavskii [9] maximized the power density of a thermionic fuel cell and obtained the optimal electrical and geometrical parameters of the cell. The optimization of a sealed nickel–cadmium battery was described by Belove and Mundel [10]. Kordesh and Clark [11] optimized the elements of construction of a hydrazine–air fuel cell, such as the cathode composition, the cell separator and the fuel concentration. Spacil and Will [12] calculated the optimal membrane thickness for a zinc–bromine battery. The design and optimization of a lithium–iron sulphide battery was reported by Shimotake *et al.* [13]. Hardt *et al.* [14] optimized the design parameters, such as the current density and the electrolyte flow rate, of a hydrazine–oxygen fuel cell for use in a zero-gravity field. The same cell was further optimized by Urbach *et al.* [15] to achieve the maximum power efficiency and operating temperature. Cnobloch *et al.* [16] calculated the optimal operating conditions of an 8 kW hydrazine–oxygen fuel cell. The optimal performance of a methanol–oxygen fuel cell was determined by Oniciu and Agachi [17], who calculated the maximum power output as a function of the electrolyte flow rate, the cell temperature and the oxygen partial pressure. Hadley and Catotti [18] optimized the overcharge capability of a nickel–cadmium cell. Alashkin *et al.* [19] optimized the reagent consumption of a hydrazine–hydrogen peroxide electrochemical power plant. The fuel utilization of an acid fuel cell was optimized by Newman [20], who presented numerical results as a function of electrode area and current density.

In the electrolysis industry, Ibl and Robertson [21] considered the use of surplus night electricity; they calculated the optimal current density for night operations in the chlor-alkali and the copper refining industries. The investment of an electrolytic copper refining process was optimized by Ibl [22], who concluded that the optimal operating current density should be greater than one-third of the limiting current density in a natural convection cell. Gallone and Messner [23] minimized the manufacturing cost for the electrolysis of hydrochloric acid. A mathematical model for the optimization of an electrolytic chlorate production cell was described by Jaksic [24].

In the present study, the operating current density, the electrolyte concentration and the cell temperature of an electrochemical hydrogen–chlorine energy storage plant have been optimized. Based on the optimal results, the design parameters of the key components in the plant are determined to yield a minimum capital investment. Although this work is specifically for the hydrogen–chlorine system, the method of mathematical modelling and the computing algorithm treated can be easily extended to the optimization of other electrochemical load-levelling and bulk energy storage systems.

2. Analysis

2.1. *Plant description*

A 20 MW/200 MW h energy storage plant is considered in this study. The plant is designed to operate with a cycle of 10 h charge and 10 h discharge. A simplified flow sheet is shown in Fig. 1. The heart of the plant is a cell stack consisting of 10 modules of 2 MW/20 MW h H_2/Cl_2 batteries; the other key components include a hydrogen clean-up and storage system, HCl/Cl_2 storage, pumps for fluid circulation and a heat exchanger for thermal conditioning. During the charge cycle, the HCl circulation pump transfers concentrated hydrochloric acid to the chlorine-electrode compartments of the cell stack, where the following reaction occurs:

$$\text{Electrical energy} + HCl(aq) = \tfrac{1}{2}H_2(g) + \tfrac{1}{2}Cl_2(l). \quad (1)$$

The Cl_2 electrode and the HCl/Cl_2 storage are pressurized at 2760 kPa (400 psi); at this pressure, the chlorine produced by the electrolysis will be in liquid form. The liquid chlorine is carried away by the excess hydrochloric acid to the HCl/Cl_2 storage where it is stored as a separate liquid phase. The hydrogen gas produced by the electrolysis is passed through a H_2 clean-up device and then stored in the H_2 storage. The SPE H_2/Cl_2 battery allows the H_2 electrode to be operated at a pressure different from the Cl_2 electrode so long as the pressure difference is less than 2760 kPa (400 psi). The cell is also capable of compressing the H_2 gas to 4100 kPa without the need of a gas compressor. In this plant layout, the hydrogen storage pressure is 690 kPa (100 psi) at the beginning of charge, and at the end of the 10 h charge cycle the H_2 pressure increases to 4100 kPa (600 psi). The hydrogen storage temperature is 298 K.

During discharge, the HCl circulation pump and the Cl_2 pump transfer the aqueous hydrochloric acid and liquid chlorine into the cell stack; the hydrogen gas also passes through the expansion valve to the H_2 electrode of the cell stack. During this period, the reverse reaction of Equation 1

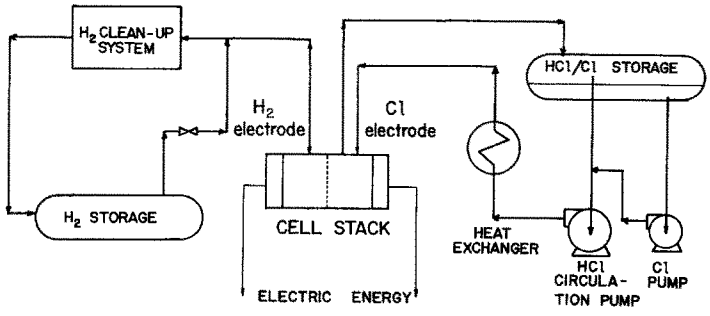

Fig. 1. Simplified flow sheet for an electrochemical hydrogen–chlorine energy storage system.

occurs. It should be noted that Equation 1 has a large entropy change; at 298 K, the value of $T\Delta S$ amounts to 8.67 kcal g-mol^{-1} HCl. This large $T\Delta S$ results in the cooling of the electrolyte during charge and a large heating effect during discharge. A typical temperature profile as calculated from the nonsteady-state heat balance [2] is shown in Fig. 2 for various cell current densities. It is seen that the electrolyte temperature decreases during the charge period; during discharge, the temperature rises rapidly due to the combined effect of $T\Delta S$ and overvoltage losses. The function of the heat exchanger is to keep the electrolyte temperature between a maximum (T_{max}) and a minimum (T_{min}) operating temperature. When the electrolyte temperature reaches T_{max}, heat will be removed from the heat exchanger to maintain the temperature at T_{max}. Conversely, when the electrolyte temperature decreases to T_{min}, heat will be added from the heat exchanger to maintain the temperature at T_{min}. The length of time required to operate the heat exchanger can be determined by the nonsteady-state heat balance; this is indicated as t_{ex} in Fig. 2.

2.2. *Objective function*

To simplify the analysis, 1.0 kW h of energy output during the discharge period will be used as the basis of calculation. The variables to be optimized are: (a) the operating cell current density (i), (b) the maximum electrolyte temperature (T_{max}), and (c) the initial electrolyte concentration X_i at the beginning of charge. These variables affect the overall electric-to-electric energy conversion efficiency, and have a great influence on the capital investment of the energy storage plant. In this analysis, the minimum electrolyte temperature T_{min}, and the final electrolyte concentration X_f at the end of the 10 h charge period will be kept at 288 K and 5 wt% HCl, respectively; this is because of environmental and techno-economic considerations [1, 2].

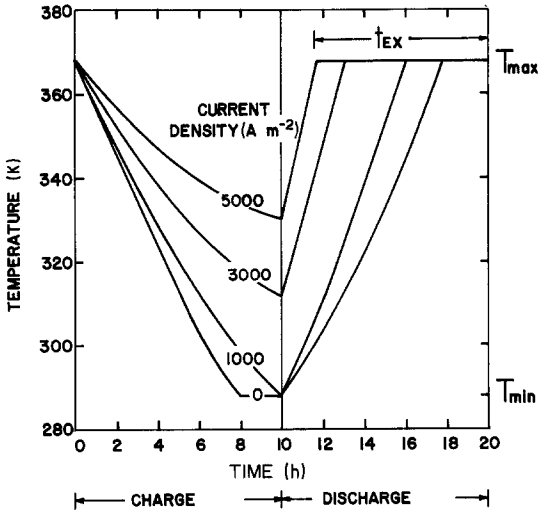

Fig. 2. Typical temperature profile for the electrolyte and cell stack. The curves were calculated for the electrolyte concentration varying from 35 wt% HCl at the beginning of charge to 5 wt% HCl at the end of the 10 h charge cycle.

According to the flow sheet shown in Fig. 1, we shall minimize the capital cost consisting of the following plant components: (a) cell stack, (b) H_2 storage, (c) HCl/Cl_2 storage, (d) heat exchanger, (e) piping and (f) pumps. The costs of installation, chemicals, the equipment for power conditioning, H_2 clean-up, sewerage, water distribution, safety precautions, etc., are not directly related to the variables to be optimized; therefore, they will not be considered in this analysis for the simplicity of mathematical formulation. The present task is to minimize the objective function $Y(i, T_{max}, X_i)$ for a 20 MW/200 MW h energy storage plant:

$$Y = \frac{\text{Cost of (cell stack + } H_2 \text{ storage + } HCl/Cl_2 \text{ storage + heat exchanger + piping + pumps)}}{\text{Net energy output during the discharge period}}$$

$$= \frac{1000 \sum_{j=1}^{6} C_{\$j} F_j^{\alpha j}}{(\int_{10}^{20} EI \, dt)_{\text{Discharge}}} \$ \, \text{kW}^{-1} \, \text{h}^{-1}. \quad (2)$$

Here $C_{\$j}$ and F_j are the cost coefficient and the design capacity of equipment j; α_j is an exponent associated with the scale-up of the equipment [25]; and E and I are the voltage and the total current from the cell stack. Equation 2 is subject to the following constraints:

$$0 \leqslant i \leqslant 5000 \, \text{A m}^{-2}$$

$$318 \, \text{K} \leqslant T_{max} \leqslant 368 \, \text{K} \quad (3)$$

$$0.05 < X_i \leqslant 0.5.$$

These values are chosen because of the availability of the cell performance data, the temperature

limitation for the plant materials to withstand the corrosion of the aqueous HCl/Cl_2 mixture, and the stability of hydrochloric acid at high temperature and concentrations. The other conditions associated with the objective function are:

$$X_f = 0.05, \quad T_{min} = 288\,K, \quad P = 2760\,kPa$$
$$P_1 = 690\,kPa, \qquad P_2 = 4100\,kPa. \quad (4)$$

2.3. *Cost estimate*

In this section, we shall summarize the cost estimate for each of the capital items listed in Equation 2. The details of the analysis are given in [26]. All the prices given below are based on a constant 1977 US dollar.

2.3.1. Cell stack. The cost of the cell stack is proportional to its electrode area A_F:

$$\text{Cost of cell stack} = C_{\$F}A_F = C_{\$F}I/i. \quad (5)$$

Here I is the total cell current, i is the operating current density, and $C_{\$F}$ is the cost coefficient per unit electrode area of the cell stack. For the General Electric SPE cell, $C_{\$F}$ has a value of $\$162\,m^{-2}$ [27].

2.3.2. H_2 storage. The hydrogen gas produced by the electrolysis will be stored in carbon steel tanks at 4100 kPa and at an ambient temperature of 298 K. The cost of storage is related to the total volume of hydrogen at the end of charge. Using the material balance, the volume can be calculated as:

$$V_{H_2} = \frac{1.87 \times 10^{-4} R(298)}{P_2 - P_1} I \quad (6)$$

where R is the universal gas constant and P_1 and P_2 are the storage pressures at the beginning and the end of the charge period, as shown in Equation 4. For a 20 MW H_2/Cl_2 energy storage plant operated with cycles of 10 h charge and 10 h discharge, V_{H_2} is approximately equal to $2600\,m^3$. The cost of the H_2 storage can be expressed as [25]:

$$\text{Cost of } H_2 \text{ storage} = C_{\$H_2} V_{H_2}^{0.53} \quad (7)$$

where the cost coefficient $C_{\$H_2}$ is equal to $\$28\,000\,m^{-1.6}$ for cylindrical carbon steel tanks [25].

2.3.3. HCl/Cl_2 storage. The design variable for this equipment is the total volume of hydrochloric acid and liquid chlorine required for the storage. It has been found that the maximum volume generally occurs at the end of charge; this volume can be determined with the material balance and the densities of the aqueous hydrochloric acid and the liquid chlorine at the end of the charge cycle [26]:

$$V_{acid} = \epsilon_{acid}\left[\left(2.54 \times 10^{-4} \frac{X_i}{X_i - 0.05} - 2.67 \times 10^{-4}\right) I + 0.0132\,(1 + \epsilon_{Cl_2}) \frac{I}{2450 - 3.6T_2}\right]. \quad (8)$$

Here T_2 is the electrolyte temperature at the end of charge; it can be determined from the nonsteady-state mass and heat balance [2]. In this study a design safety factor of $\epsilon_{acid} = 1.1$ and a fractional excess of liquid chlorine, $\epsilon_{Cl_2} = 0.2$, will be used. The HCl/Cl_2 storage will be of a glass-lined steel tank of approximately $900\,m^3$. The cost estimate for this equipment is [28]:

$$\text{Cost of } HCl/Cl_2 \text{ storage} = C_{\$acid} V_{acid}^{0.48} \quad (9)$$

where the cost coefficient $C_{\$acid}$ is equal to $\$21\,300\,m^{-1.4}$ [29].

2.3.4. Heat exchanger. The function of the heat exchanger is to remove the waste heat during discharge and to limit the electrolyte and cell temperature within the operating limits. The amount of heat $-Q_{ex}$ to be removed through the heat exchanger is determined from the nonsteady-state mass and heat balance [2]; it is a function of the operating current density i, the maximum electrolyte temperature T_{max}, and the initial electrolyte concentration X_i at the beginning of charge:

$$Q_{ex} = Q_{ex}(i, T_{max}, X_i). \quad (10)$$

The cost of the heat exchanger depends upon the design heat-transfer area A_{ex}, which can be calculated according to:

$$A_{ex} = -\frac{Q_{ex}}{t_{ex} U_{ex} (T_{max} - T_c)}. \quad (11)$$

Here T_c is the average cooling water temperature; an ambient temperature of 298 K will be used for the calculation. The quantity t_{ex} is the length of time for the heat exchange operation; it is deter-

mined with the nonsteady-state mass and heat balance. The quantity U_{ex} is the overall heat transfer coefficient; according to Ludwing [30], a value of $U_{ex} = 3.07 \times 10^6$ J h^{-1} m^{-2} K^{-1} can be used for design purposes. In this study, a tantalum heat exchanger will be used to handle the corrosive solution of HCl and Cl_2. The cost of the heat exchanger can be estimated as [28]:

$$\text{Cost of heat exchanger} = C_{\$ex} A_{ex}^{0.94} \quad (12)$$

where $C_{\$ex}$ has a value of \$5000 m$^{-1.9}$ for a size of A_{ex} of the order of 300 m^2 [29].

2.3.5. Piping. We shall only consider the pipes for the circulation of the electrolyte. The piping cost for the transport of hydrogen gas has been estimated to be less than \$1.35 kW^{-1} h^{-1} [31]; it is independent of the operating conditions and can be neglected in this analysis. The pipeline to transport the electrolyte consists of glass-lined steel pipes of 0.0394 m (10 in) inside diameter; the pipeline is estimated to be 300 m long [31]. A flow rate which enables a maximum of 30% conversion of dissolved Cl_2 in the HCl electrolyte during the discharge period will be used for the design purpose. For the 20 MW/200 MW h plant, this flow rate is rather large, and several parallel pipelines will be required. The cost of the pipelines can be determined by:

$$\text{Cost of pipe} = NC_{\$pipe}L. \quad (13)$$

Here N is the number of parallel pipelines; the cost coefficient $C_{\$pipe}$ is equal to \$290 m^{-1} [29] for the 0.0394 m internal diameter glass-lined steel pipes; and L is the pipeline length of 300 m. Using the material balance, the design flow rate can be evaluated from the following relation:

$$G_D = \max\left(\frac{6.23 \times 10^{-5} I}{S_{Cl_2}}\right). \quad (14)$$

Here S_{Cl_2} is the solubility of chlorine in aqueous HCl; it is a function of temperature, HCl concentration and the system pressure [2]. Equation 14 can be evaluated from the nonsteady-state mass and heat balance, and the number of parallel pipelines is related to G_D by

$$N = \text{integer}\left(\frac{G_D}{\frac{1}{4}\pi(0.0394)^2 3600 V} + 1\right). \quad (15)$$

Here V is the design linear velocity for the flow of electrolyte; a value of 1.5 m s^{-1} [30] is usually chosen for the design purposes. It can be estimated that approximately a total of eight pipelines will be needed.

2.3.6. Pumps. A tantalum centrifugal pump will be used to recirculate the electrolyte. The Cl_2 pump is a PTFE-lined metering pump with a double Teflon diaphram; it is estimated that each pump costs \$47 600 [29, 31]. The cost of the HCl pump depends upon its design brake power; using a macroscopic mechanical energy balance, the design brake power can be estimated as:

$$W_P = \frac{3.12 \times 10^{-4}}{\eta_p} \bar{\rho}_{HCl} (G_D/N)^3 \quad (16)$$

where $\eta_p = 0.8$ is the pump efficiency and $\bar{\rho}_{HCl}$ is the average density of the hydrochloric acid electrolyte over the discharge period. A Reynolds number of 2×10^5, a fanning friction factor of 0.004, a pipeline length of 300 m, and a 10% of additional frictional loss through valves, elbows, and other pipe fittings have been taken into account in the numerical coefficient of Equation 16 [26]. The total cost for N HCl pumps and N Cl_2 pumps is [32]:

$$\text{Costs of pumps} = NC_{\$pump} W_p^{0.98} + 47600N \quad (17)$$

where the cost coefficient $C_{\$pump}$ for an average 7.5 kW tantalum pump is \$1.7 (J/s)$^{-0.98}$.

2.4. *Nonsteady-state mass and energy balance*

The operation of the electrochemical H_2/Cl_2 energy storage system is a time-dependent process. The nonsteady-state mass and heat balance permits one to determine the changes in the electrolyte concentration, the electrolyte temperature and the cell voltage during the charge and discharge operations; it also permits one to calculate the amount of waste heat $-Q_{ex}$ to be removed, and the length of time t_{ex} required for the heat exchange operation. Once the temperature and the concentration of the electrolyte are determined, one can further proceed to calculate the design flow rate G_D from Equation 14, and the average electrolyte density $\bar{\rho}_{HCl}$ required for the calculation of the pumping brake power (Equation 16). The details of the mathematical formulation are given in [2]. For the present system, shown in Fig. 1, a

material and energy balance between time t_0 and t results in the following governing equations:

$$-3600\int_{t_0}^{t} EI\,\mathrm{d}t - 2.02\frac{\Delta n_{HCl}}{2} \times \int_{T}^{298} C_{v,H_2}\,\mathrm{d}T + Q_{ex} = W_{HCl,0}\int_{T_0}^{298} C_{p,HCl}\mathrm{d}T + W_{Cl_2,0} \times \int_{T_0}^{298} C_{p,Cl_2}\,\mathrm{d}T + \Delta n_{HCl}H^0_{f,HCl}(X) + \frac{X_0 W_{HCl,0}}{36.5}[H^0_{f,HCl}(X) - H^0_{f,HCl}(X_0)] - \frac{\Delta n_{HCl}}{2}H^0_{f,Cl_2} + (W_{Cl_2,0} - \tfrac{71}{2}\Delta n_{HCl}) \times \int_{298}^{T} C_{p,Cl_2}\,\mathrm{d}T + (W_{HCl,0} + 36.5\Delta n_{HCl}) \times \int_{298}^{T} C_{p,HCl}\mathrm{d}T \quad (18)$$

$$\Delta n_{HCl} = \mp\frac{3600}{F}\int_{t_0}^{t} I\mathrm{d}t \quad (19)$$

$$W_{HCl} = W_{HCl,0} + 36.5\Delta n_{HCl} \quad (20)$$

$$W_{Cl_2} = W_{Cl_2,0} - 71\frac{\Delta n_{HCl}}{2} \quad (21)$$

$$X = \frac{W_{HCl,0}X_0 + 36.5\Delta n_{HCl}}{W_{HCl,0} + 36.5\Delta n_{HCl}} \quad (22)$$

$$Q_{ex} = 0 \qquad \text{for } T_{min} < T < T_{max}. \quad (23)$$

The quantities with subscript 0 are variables and physical and thermodynamical properties at time t_0; those without the subscript 0 are the instantaneous variables and properties at time t. The convention used here is that the cell voltage E and Δn_{HCl} have negative values during charge and positive values during discharge. The function of Q_{ex} is to regulate the electrolyte temperature within the operating limits as discussed before. The values of C_{p,H_2}, $C_{p,HCl}$, C_{p,Cl_2}, $H^0_{f,HCl}$, H^0_{f,Cl_2}, ρ_{HCl}, and S_{Cl_2} have been summarized elsewhere [2, 26, 33–36]. The E versus i curves for the General Electric SPE cells have been previously reported [4]; the test data can be summarized by the following empirical equations:

For charge

$$E = -[1.28 - 0.96(X - 0.1) - 0.0017(T - 298) + 4.3 \times 10^{-5}T(\ln P - 4.62) + 9.87 \times 10^{-6}P] - [0.78 - 0.006(T - 298)] \times 10^{-4}i. \quad (24)$$

For discharge

$$E = 1.28 - 0.96(X - 0.1) - 0.0017(T - 298) + 4.3 \times 10^{-5}T(\ln P - 4.62) + 9.87 \times 10^{-6}P - (4.54 - 0.011\,T) \times [1 + 1.07\exp(-0.0087P)] \times 10^{-4}i \quad (25)$$

where P is the cell pressure in kPa and T is the electrolyte temperature in K. Equations 18–25 can be used to calculate the cell voltages during the charge and the discharge cycles, and the overall electric-to-electric efficiency for energy storage may then be evaluated as follows:

$$\epsilon(\%) = -\frac{3600(\int_{10}^{20} EI\,\mathrm{d}t)_{discharge} - H_m}{3600(\int_{0}^{10} EI\,\mathrm{d}t)_{charge}} \times 100. \quad (26)$$

Here H_m is the total mechanical energy losses, consisting of the energy consumed by pumping the electrolyte and the cooling water during the charge and the discharge cycles. It has been found that the value of H_m amounts to only 0.4 MW h in the present system [26]; this value is small as compared with the integral of EI during discharge, and may be neglected for most calculations.

3. Numerical results and discussion

3.1. *Characteristics of the objective function*

A constant current of 2×10^7 A has been used as the basis of numerical computation. To calculate the objective function Y, one needs to substitute Equations 5–17 into Equation 2 and to carry out the integration of EI over the discharge period. A 'golden ratio' search method [37, 38] has been used to solve Equations 18–26 for the cell voltage E, the electrolyte temperature T, the waste heat $-Q_{ex}$, the length of time for the heat exchange operation t_{ex}, the design flow rate of the electrolyte G_D, the average electrolyte density $\bar{\rho}_{HCl}$, and the overall electric-to-electric efficiency ϵ. These quantities are then used in Equations 2–17

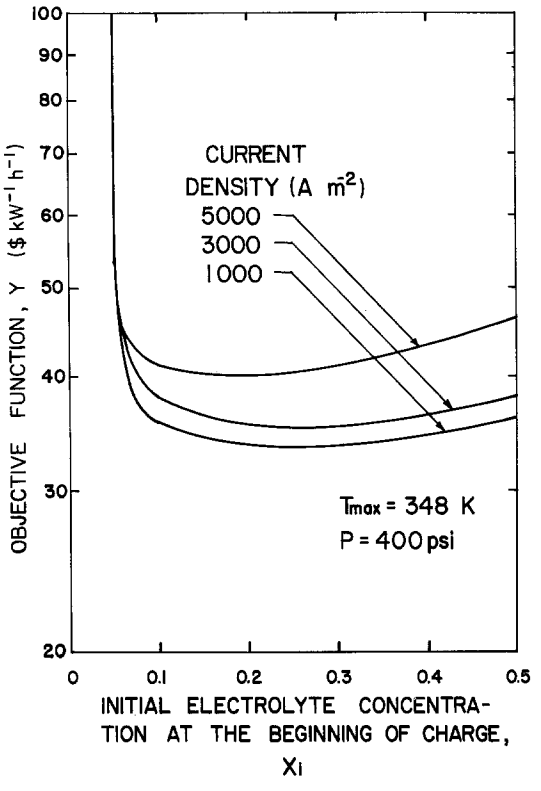

Fig. 3. The objective function Y versus X_i for various operating current densities at $T_{max} = 348$ K.

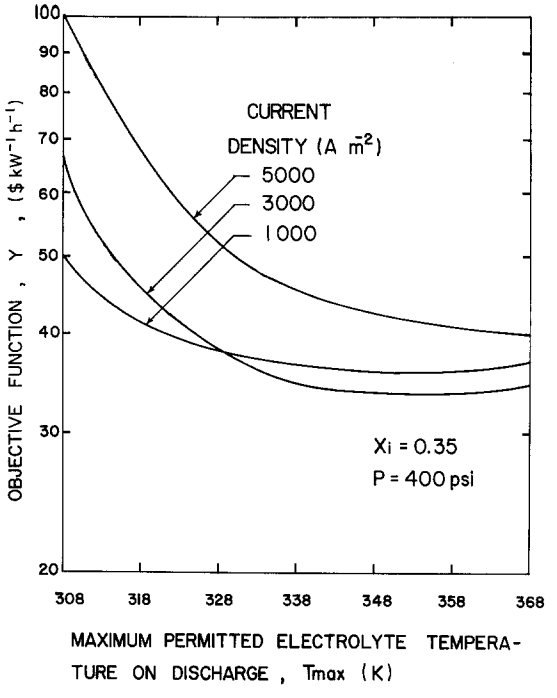

Fig. 4. The objective function Y versus T_{max} for various operating current densities at $X_i = 0.35$.

for the numerical evaluation of the objective function Y.

In Fig. 3, the values of Y are plotted against the electrolyte concentration at the beginning of charge X_i for the various operating current densities i; these curves are calculated for a given maximum operating temperature of $T_{max} = 348$ K. The curves show a sharp decrease in the value of Y as X_i starts to deviate from the final electrolyte concentration of $X_f = 0.05$, apparently caused by a decrease in the cost of the HCl/Cl_2 storage as X_i increases. The curves go through a minimum in the region of $0.15 < X_i < 0.35$ and then increase with further increase in X_i, due to a decrease in the electric-to-electric efficiency at high electrolyte concentrations. The effect of T_{max} on the objective function is shown in Fig. 4, where the curves for various i are obtained at $X_i = 0.35$. It is seen that as T_{max} increases, the value of Y decreases primarily due to a decrease in the required heat exchange area, as shown in Equation 11. The influence of the operating current density i is shown in Figs. 5 and 6 for various T_{max}

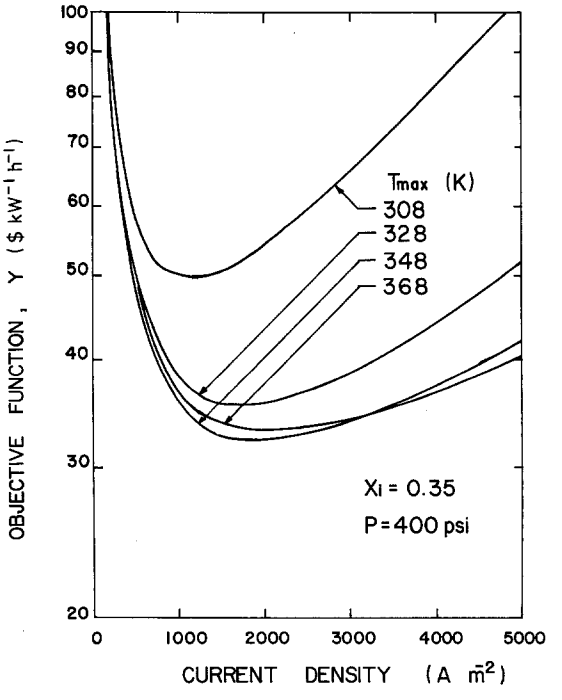

Fig. 5. The objective function Y versus i for various T_{max} at $X_i = 0.35$.

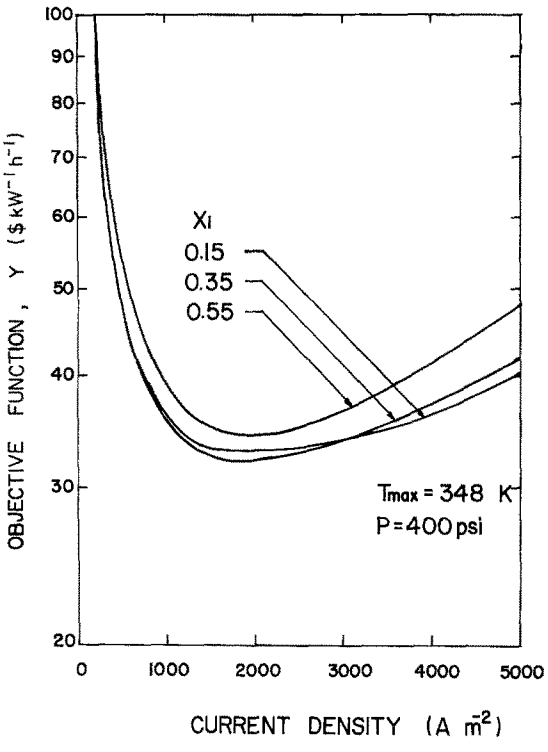

Fig. 6. The objective function Y versus i for various X_i at $T_{max} = 348$ K.

and X_i. The objective function is shown to decrease with increasing i in the low current density region, reach a minimum, and then increase with further increasing i in the high current density region. The initial decrease in Y is caused by a decrease in the cost of the cell stack as the operating current density increases. However, this decrease is offset by a decrease in the electric-to-electric efficiency, and the need for a larger heat exchanger at high current densities. In addition, the electrolyte temperature is higher at high operating current densities. This causes a decrease in the solubility of chlorine in the electrolyte, and a larger pumping rate will be required to recirculate the electrolyte to meet the requirement of 30% conversion in the cell stack. Consequently the value of Y increases with i in the region of high current densities.

3.2. *Optimization results*

Figs. 3–6 indicate that there is a minimum for the objective function in the region: $0.15 < X_i < 0.35$, $338\,K < T_{max} < 368\,K$ and $1000\,A\,m^{-2} < i < 2500\,A\,m^{-2}$. Using Hooke and Jeeve's direct search method [39], a computer program has been prepared to locate the optimal point [26]. The results of the numerical computation are given in Table 1. The optimal point is found to be at: $X_i = 0.3$, $T_{max} = 343$ K and $i = 1900\,A\,m^{-2}$. The associated profiles for the electrolyte temperature and the cell voltage are shown in Fig. 7. It is seen that under the optimal operating conditions, the cell voltage increases from 1.16 V to 1.52 V during charge and decreases from 1.12 V to 0.9 V during discharge. The electrolyte temperature decreases from $T_{max} = 343$ K at the beginning of charge to $T_2 = 296$ K at the end of charge; during discharge,

Table 1. Results of the optimization calculation

Item	*Capital cost* ($\$\,kW^{-1}\,h^{-1}$)	*Percentage*	*Design capacity*
Cell stack	8.5	26.6	1.05×10^4 m² cell area
H_2 storage	9.5	29.8	2.68×10^3 m³ storage volume
HCl/Cl_2 storage	3.1	9.7	1.07×10^3 m³ storage volume
Heat exchanger	6.0	18.8	2.81×10^2 m² heat exchanger area
Pump	1.8	5.6	2.4×10^3 J s^{-1} pump brake power
Piping	3.0	9.5	7 parallel pipelines
Total cost	31.9	100.0	

Optimal operating condition:
$i = 1900\,A\,m^{-2}$, $T_{max} = 343$ K (70° C), $X_i = 0.3$, $\epsilon = 74.6\%$

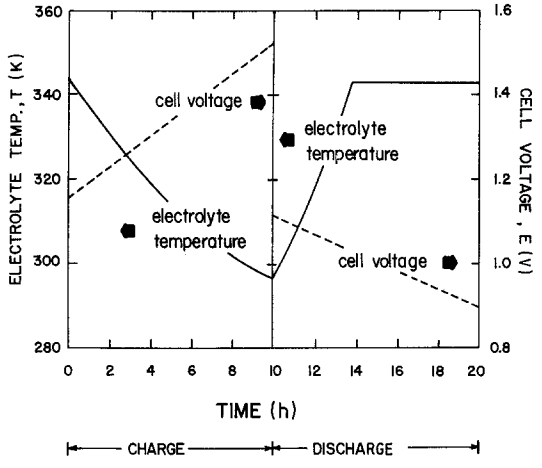

Fig. 7. The temperature profile and the cell voltage at the optimal operating condition of $i = 1900\ \mathrm{A\,m^{-2}}$, $T_{max} = 343\ \mathrm{K}$ and $X_i = 0.3$.

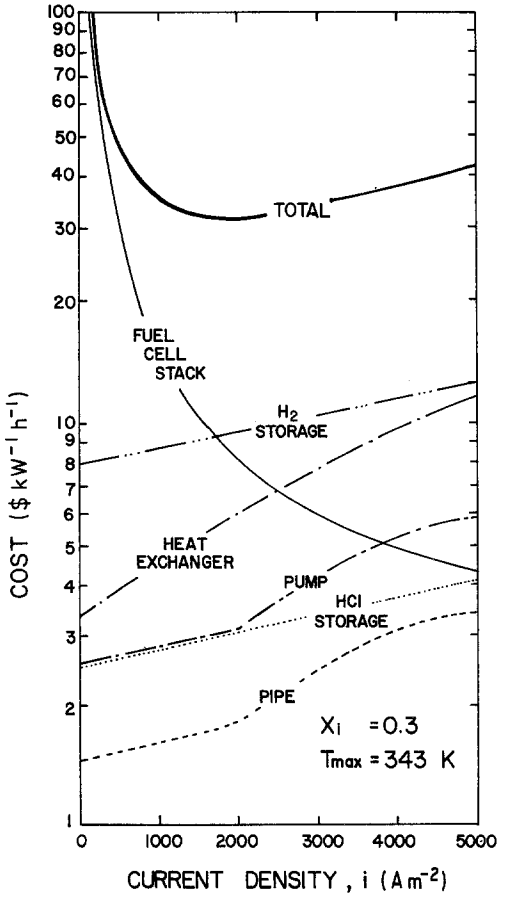

Fig. 8. Capital investment cost as a function of i at the optimal $T_{max} = 343\ \mathrm{K}$ and $X_i = 0.3$.

it increases back to $T_{max} = 343\ \mathrm{K}$ at $t = 13.75\ \mathrm{h}$. The total input electric energy during the charge cycle is 268 MW h, and the net output electric energy during the discharge cycle is 200 MW h, this yields an overall electric-to-electric efficiency of $\epsilon = 74.6\%$. The total electrode area required for the cell stack to operate at the optimal condition is $10\,500\ \mathrm{m^2}$. The design volumes for the H_2 storage and the HCl/Cl_2 storage are $2680\ \mathrm{m^3}$ and $1070\ \mathrm{m^3}$, respectively. The waste heat to be removed during the discharge cycle is 2.4×10^{11} J (5.7×10^7 kcal); this requires a heat exchange area of $281\ \mathrm{m^2}$. Also, a total of seven pipelines, and seven sets of Cl_2 pumps and HCl pumps will be needed to recirculate the electrolyte at a rate of $1880\ \mathrm{m^3\ h^{-1}}$ (8280 gal $\mathrm{min^{-1}}$); the brake power required for each HCl pump is $2400\ \mathrm{J\,s^{-1}}$ (4 HP).

The minimum cost for the six capital items included in Equation 2 is $\$31.9\ \mathrm{kW^{-1}\ h^{-1}}$, columns 2 and 3 in Table 1 list the cost-breakdown for each item. In Fig. 8, the total capital cost and the capital cost of each item are plotted as a function of the operating current density at the optimal $T_{max} = 343\ \mathrm{K}$ and $X_i = 0.3$. It can be seen that the capital costs of each item except the cell stack increase as the operating current density increases. Only the cost of the cell stack decreases as the operating current density increases. The influence of the current density on the cost of H_2 storage and HCl/Cl_2 storage is due to a decrease in the electric-to-electric efficiency as previously mentioned. The influence of current density on the cost of heat exchanger, pump, and piping is due to a combined effect of decreasing the electric-to-electric efficiency and increasing the design flow rate of the electrolyte. The major cost items in the objective function are the cell stack, the H_2 storage, and the heat exchanger, which constitute 75% of the total capital investment, as shown in Table 1.

3.3. *Sensitivity tests*

Since the purchasing costs of equipment change with time, a sensitivity test on the cost coefficient $C_{\$j}$ will give an idea of the changes in the optimal operating condition with changing equipment purchase prices. Fig. 9 shows a sensitivity test of the cost coefficient of the cell stack $C_{\$F}$. It should be noted that a value of $C_{\$F} = \$162\ \mathrm{m^{-2}}$ has been used in the present optimization calculations: a

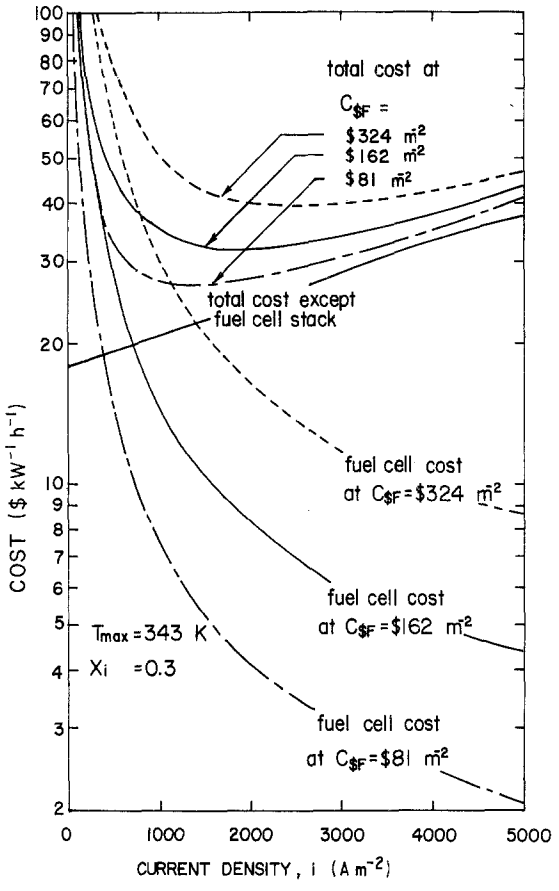

Fig. 9. Sensitivity test for the cost coefficient $C_{\$F}$ of the cell stack.

cell cost curve for $C_{\$F} = \$162\,m^{-2}$ is shown in the figure. Two additional cell cost curves are also plotted in the figure: one is for $C_{\$F} = \$81\,m^{-2}$ and the other is for $C_{\$F} = \$324\,m^{-2}$. The sum of the capital costs for the remaining five items are shown as a single line. It is seen that as the cost coefficient of the cell stack changes from $\$162\,m^{-2}$ to $\$324\,m^{-2}$ the influence of the cost of the cell stack on the total capital investment becomes more important. This forces the optimal operating current density at $C_{\$F} = \$324\,m^{-2}$ to a higher value than for $C_{\$F} = \$162\,m^{-2}$. The optimal operating current density changes from $i = 1900\,A\,m^{-2}$ to $i = 2500\,A\,m^{-2}$ as $C_{\$F}$ changes from $\$162\,m^{-2}$ to $\$324\,m^{-2}$. On the other hand, as the cost coefficient of the fuel cell stack changes from $C_{\$F} = \$162\,m^{-2}$ to $C_{\$F} = \$81\,m^{-2}$, the influence of the cost of the fuel cell stack on the total capital investment becomes less important. Thus the optimal operating current density changes from $i = 1900\,A\,m^{-2}$ to $i = 1400\,A\,m^{-2}$ as $C_{\$F}$ changes from $\$162\,m^{-2}$ to $\$81\,m^{-2}$.

A similar test has been made for the cost coefficient of H_2 storage, $C_{\$H_2}$ [26]. It can be shown that the minimum capital investment changes from $\$31.9\,kW^{-1}\,h^{-1}$ to $\$41\,kW^{-1}\,h^{-1}$ as $C_{\$H_2}$ changes changes from $\$28\,000\,m^{-1.6}$ to $\$56\,000\,m^{-1.6}$, and from $\$31.9\,kW^{-1}\,h^{-1}$ to $\$27\,kW^{-1}\,h^{-1}$ as $C_{\$H_2}$ changes from $\$28\,000\,m^{-1.6}$ to $\$14\,000\,m^{-1.6}$.

3.4. *Comparison of plant erection costs between optimal and unoptimized designs*

A cost assessment of a 20 MW/200 MW h electrochemical hydrogen–chlorine energy storage plant has been made by Oronzio de Nora Impianti Elettrochimici SpA [31]. The plant was designed for a specific operating condition of $i = 2250\,A\,m^{-2}$, $T_{max} = 368\,K$ and $X_i = 0.35$, with an overall electric-to-electric energy conversion efficiency of 67%. Using their cost data, a comparison for the plant erection costs is given in Table 2. The figures in the table do not include the land costs and are based on 1.0 kW h of output electric energy from the plant during the discharge period. It is seen that the key plant components included in the objective function constitute a major contribution to the total plant erection cost. The optimal operating conditions not only increase the electric-to-electric efficiency from 67% to 75% but also results in a reduction of the plant erection cost from $\$109.8\,kW^{-1}\,h^{-1}$ to $\$88.7\,kW^{-1}\,h^{-1}$. Based on a 200 MW h energy output, the optimization decreases the erection costs from $21.96 million to $17.75 million; this represents a net saving of $4.21 million. No life-time tests have, however, been reported for the hydrogen–chlorine energy storage system and the optimal operating conditions should also take the results of such tests into account.

4. Conclusions

Using a nonsteady-state mass and heat balance, a mathematical model has been presented for the optimization of an electrochemical hydrogen–chlorine energy storage system. Numerical calculations have been made to minimize the capital investment of a 20 MW/200 MW h plant operated on a cycle of 10 h charge and 10 h discharge. Based on the existing data for the cell performance, the

Table 2. Cost comparison between the optimized and unoptimized operating conditions (basis $ kW^{-1} h^{-1})

		Optimized	*Unoptimized [31]*
(a) Materials			
(i) Chemicals H_2		$ 0.01	$ 0.01
Cl_2		0.17	0.17
(ii) Equipment			
Key components	Fuel cell stack	8.5	
	Hydrogen storage	9.5	
	HCl/Cl_2 storage	3.1	
	Heat exchanger	6.0	
	Pump	1.8	
	Pipe	3.0	
	Sub-total	31.90	53.00
Safety facilities		3.45	3.45
Other utilities	Compressed air and H_2O Generation and distribution Sewerage Extra HCl storage	9.91	9.91
Metallic structure		1.65	1.65
Instruments		1.64	1.64
Plant electric power and network and motors		0.83	0.83
Sub-total		49.56	70.66
(b) Erection labour		19.73	19.73
(c) Engineering fees		12.08	12.08
(d) A.c./d.c. power condition		7.36	7.36
Total		$88.73	$109.83
(e) Operating conditions			
Current density (A m^{-2})		1900	2250
T_{max} (K)		343	368
X_i		0.3	0.35
(f) Overall electric-to-electric efficiency (%)		75.0	66.6

cost assessment and the physical and the thermodynamical properties, the optimal operating parameters are found to be: $i = 1900$ A m^{-2}; $T_{max} = 343$ K and $X_i = 0.3$. Under these conditions the plant will be 75% efficient, and the capital cost for the key plant components is $31.9 kW^{-1} h^{-1}. This result is a 20% reduction in the total plant erection cost, as compared to the unoptimized case.

Acknowledgements

Special thanks are due to Dr R. S. Yeo of the Continental Group Inc, Mr J. F. McElroy of General Electric Company, and Dr P. M. Spaziante and Mr A. Perego of Oronzio de Nova Impianti Elettrochimici SpA for their technical assistance and helpful discussions. This work was carried out under the auspices of the United States Department of Energy.

References

[1] E. Gileadi, S. Srinivasan, F. J. Salzano, C. Braun, A. Beaufrere, S. Gottsfeld, L. J. Nuttal and A. B. LaConti, *J. Power Sources* 2 (1977) 191.
[2] D.-T. Chin, R. S. Yeo, J. McBreen and S. Srinivasan, *J. Electrochem. Soc.* **126** (1979) 713.
[3] R. S. Yeo and J. McBreen, *J. Electrochem. Soc.* **126** (1979) 1682.
[4] R. S. Yeo, J. McBreen, A. C. C. Tseung, S. Srinivasan and J. McElroy, *J. Appl. Electrochem.* in press.
[5] R. S. Yeo and D.-T. Chin, *J. Electrochem. Soc.* **127** (1977) 549.
[6] D. Lucesoli and P. Degobert, *Ann. Combust. Liquides* **25** (1970) 1037.

[7] A. P. Sharaevskii, L. I. Stolyarenko and V. A. Kasatkina, *Industrial Laboratory* 38 (1972) 411.
[8] J. Ceynowa and R. Wodzki, *J. Power Sources* 1 (1976) 323.
[9] Y. A. Brovalskii and V. V. Sinyavskii, *Sov. Phys. Tech. Phys.* 17 (1973) 1530.
[10] L. Belove and A. B. Mundel, *Proc. 22nd Power Sources Symp.*, The Electrochemical Society, Princton, N.J. (1968) pp.46–50.
[11] K. V. Kordesch and M. B. Clark, *Proc. 24th Power Sources Symp.*, The Electrochemical Society, Princtone, N.J. (1970) p.207.
[12] H. S. Spacil and F. G. Will, *Proc. Symp. on Battery Design and Optimization*, Vol. 79–1 The Electrochemical Society, Princeton, N.J. (1979) p.222.
[13] H. Shimotake, E. C. Gay and P. A. Nelson, *ibid* (1979) p.408.
[14] A. P. Hardt, H. M. Cota, J. L. Fick and T. Katan, *Electrochim. Acta* 8 (1963) 815.
[15] H. B. Urbach, D. E. Icenhower and R. J. Bowen, *Proc. 25th Power Source Symp.*, The Electrochemical Society, Princeton, N.J. (1972) p.182.
[16] H. Cnobloch and H. Kohlmueller, *Chem. -Ztg.* 97 (1973) 502.
[17] L. Oniciu and S. Agachi, *Ser. Chem.* 19 (1974) 76.
[18] R. L. Hadley and A. J. Catotti, *Proc. 22nd Power Sources Symp.*, The Electrochemical Society, Princeton, N.J. (1968) p.42.
[19] V. M. Alashkin, B. P. Nesterov and N. V. Korovin, *Electrokhimiya* 13 (1977) 311.
[20] J. Newman, *Electrochim. Acta* 24 (1979) 223.
[21] N. Ibl and P. M. Robertson, *Electrochim. Acta* 18 (1973) 897.
[22] N. Ibl, *ibid* 22 (1977) 465.
[23] P. Gallone and G. Messner, *Electrochem. Technol.* 3 (1965) 321.
[24] M. M. Jaksic, *Electrochim. Acta* 21 (1976) 1127.
[25] M. S. Peters and K. D. Timmerhaus, 'Plant Design and Economics for Chemical Engineers', McGraw-Hill, New York (1968).
[26] K. L. Hsueh, MS Thesis, Clarkson College of Technology, Potsdam, New York (1979).
[27] J. McElroy, 'Hydrogen–Halogen Energy Storage Systems Development', Phase I Summary Report, Contract No. 410127-S, General Electric Co., Direct Energy Conversion Programs, Wilmington, Massachussetts (1977).
[28] G. S. G. Beveridge and R. S. Schechter, 'Optimization Theory and Practice', McGraw-Hill, New York (1970).
[29] A. Perego, private communication, Oronzio de Nora Impianti Elettrochimici SpA, Milano, Italy (1979).
[30] E. E. Ludwing, 'Applied Process Design for Chemical Plants', Gulf Publishing Co., Houston, Texas (1965).
[31] P. M. Spaziante, G. C. Sioli, R. Trotta and A. Perego, 'Hydrogen/Chlorine Energy Storage System Safety Assessment and Plant Cost Estimate', Final Report on BNL contract No. 451857-S, ODN Job No. 018/BNL, Oronzio de Nora Impianti Elettrochimici SpA, Milano, Italy (1979), Brookhaven National Laboratory Upton N.Y. Report No. BNL-51070.
[32] A. Pikulick and H. E. Diaz, *Chem. Eng.* 21:84 (1977) 106.
[33] J. C. Bailer, H. J. Emeleus, S. R. Nyholm and A. F. Trotman-Dickenson, 'Comprehensive Inorganic Chemistry', Pergamon Press, New York (1973).
[34] R. H. Perry, 'Chemical Engineering Handbook' 5th edn, McGraw-Hill, New York (1973).
[35] E. W. Washburn, 'International Critical Tables of Numerical Data, Physics, Chemistry and Technology', 1st edn, Vol. 5, McGraw-Hill, New York (1929).
[36] J. W. Mellor, 'A Comprehensive Treatise on Inorganic and Theoretical Chemistry, Supplement II, Part I', Longmans, Green Co., New York (1956).
[37] B. S. Gottfried and J. Weisman, 'Introduction to Optimization Theory', Prentice-Hall, Englewood Cliffs, New Jersey (1973).
[38] J. L. Kuester and M. H. Mize, 'Optimization Techniques with Fortran', McGraw-Hill, New York (1973).
[39] R. Hooke and T. A. Jeeves, *J. Assoc. Computer Machines* 8 (1961) 212.